Audio Engineering Society

Convention Paper 10542

Presented at the 151st Convention
2021 October, Online

Analyzing a Unique Pingable Circuit: The Gamelan Resonator

Kurt James Werner[1] and Ezra J. Teboul[2]

[1]*iZotope, Inc., Cambridge, MA, 20141, USA*

[2]*Paris, France*

Correspondence should be addressed to (kwerner@izotope.com and ezra@redthunderaudio.com)

ABSTRACT

This paper offers a study of the circuits developed by artist Paul DeMarinis for the touring version of his work *Pygmy Gamelan*. Each of the six copies of the original circuit, developed June-July 1973, produce a carefully tuned and unique five-tone scale. These are obtained by five resonator circuits which pitch pings produced by a crude antenna fed into clocked bit-shift registers. While this resonator circuit may seem related to classic Bridged-T and Twin-T designs, common in analog drum machines, DeMarinis' work actually presents a unique and previously undocumented variation on those canonical circuits. We present an analysis of his third-order resonator (which we name the *Gamelan Resonator*), deriving its transfer function, time domain response, poles, and zeros. This model enables us to do two things: first, based on recordings of one of the copies, we can deduce which standard resistor and capacitor values DeMarinis is likely to have used in that specific copy, since DeMarinis' schematic purposefully omits these details to reflect their variability. Second, we can better understand what makes this filter unique. We conclude by outlining future projects which build on the present findings for technical development.

1 Introduction

Paul DeMarinis (born 1948) is an artist and teacher working with electronics and sound. This paper focuses on one of his early works, developed at the beginning of his time in David Tudor's *Composers Inside Electronics* group. Originally designed in 1973, the *Pygmy Gamelan* has a number of versions with varying levels of documentation. In its original instances (see Fig. 1), stray electromagnetic fields are fed into two 8-bit shift registers which trigger tuned resonators to ring at specific frequencies. Each is tuned to a different set of five tones, with these pentatonic scales then playing autonomously and side by side in gallery contexts. In later iterations of the device, the pattern generation circuits varied greatly: "Each unit has a unique pitch set and different rhythmic scheme. The second edition had much more varied logic sequencers beyond the TTL shift register, including one that used the RCA CMOS 1-bit microprocessor!"[1]. This installation is mentioned in a number of interviews [2, 3, 4, 5], but remained relatively unstudied prior to 2020 [6].

Although it had originally been included in the journal *Asterisk* [1], DeMarinis uploaded the *Pygmy Gamelan* circuit schematic on his website in the 2010s [7]. A condensed version is re-drawn in Fig. 2. In coordination with a recording of the 1978 piece *Forest Booties* which features one of those devices [8], the schematic

[1] email with Paul DeMarinis, 6/4/2019

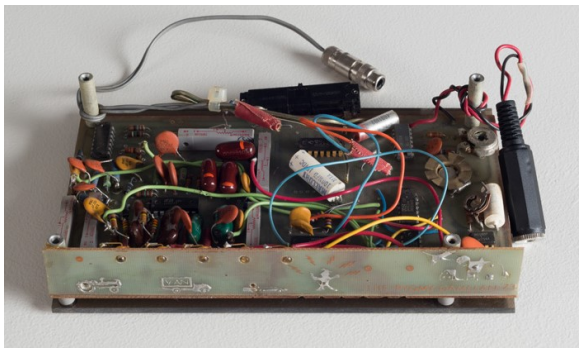

Fig. 1: Paul DeMarinis, *Pygmy Gamelan* (detail), 1973. Electronics, plexiglass and speaker. $1.5 \times 7 \times 4.5$ inches. Gift of the Kathryn C. Wanlass Foundation. Image courtesy of the Nora Eccles Harrison Museum of Art, Utah State University.

makes it possible to understand exactly how technical decisions made before and during the assembly of each iteration of the original set of devices affected the artistic experience of witnessing a performance. Indeed, DeMarinis carefully tuned each of the six copies of this circuit based on available components and harmony, both with itself and with the other instances.[2]

Here we develop work originally presented in [6] to better understand how DeMarinis' unique filter design shapes the timbres produced by his system. In §2, we describe the circuit, and comment on how it can be reasonably separated into sub-circuits to simplify analysis. In §3, we model the Norton amplifier as an ideal amplifier (a nullor), and show that this is not sufficient to describe the device's behavior because it is only marginally stable (while the real devices are stable). In §4, we model the Norton amplifier as a finite-gain voltage-controlled voltage source (VCVS), yielding a stable resonator, and analyze this unique circuit in terms of its frequency response, time-domain response, zeros, and poles. §5 shows how theoretical knowledge of the circuit can be combined with historical context and the *Forest Booties* recording to calculate possible component values experimentally. §6 discusses potential digital modeling and simulation strategies. §7 concludes.

[2]For a discussion of the experimental process behind these tunings and their relationships to preexisting scales, see [6, pp. 72–75]

2 Gamelan Resonator Circuit

2.1 Presentation

The *Pygmy Gamelan* schematic is shown in Fig. 2. Five streams of voltage pulses generated by the clocked shift registers and antennae drive five filter subcircuits tuned to a unique frequency. These five voices are summed together by a summing amplifier and drive a speaker.

Conceptually, each of the five voices can be broken into two parts: a pulse shaper that alters the rectangular pulses generated by the shift registers, and a resonator circuit, see Fig. 4. This division of a circuit into pulse generation, pulse shaping, and resonators is extremely common in analog drum machine circuits, such as the Roland TR-808 [9, 10, 11, 12].

Analog drum machines typically use passive inductor–capacitor "tanks," phase-shift oscillators tuned just below oscillation, or active filters with a high Q as their resonator. The two main designs used in classic analog drum machines are the Twin-T and Bridged-T networks, which form resonators by taking a passive Twin-T or Bridged-T resistor-capacitor network (a very old type of circuit, e.g., [13, 14]) and adding active feedback around the network.

DeMarinis's resonator, which we'll call the *Gamelan Resonator* (GR), comprises three resistors (two of identical value R and one of value $R/12$), three identical capacitors C and a Norton operational amplifier. The LM3900 Norton amplifier is an unusual integrated circuit, having even been called "inelegant" [15]. Nevertheless, it appears in a number of audio synthesis circuits. As an input, the Gamelan Resonator takes a current i_{in}. Its output is taken as the Norton operational amplifier's output voltage.

The GR bears a resemblance to the classic Bridged-T and Twin-T resonators (shown side-by-side in Fig. 3), but is a distinct and seemingly completely unique design. A survey of many dozens of analog drum circuits, active filter design textbooks, circuit theory research articles, and op-amp and Norton amplifier datasheets turns up nothing with a similar topology, let alone the specific arrangement of resistor and capacitor values. Our attempts to find a source for the GR uncovered only two leads:

First, Paul DeMarinis recalls working off of a design by Ralph Burhans,[3] described in the May 1973 JAES

[3]email with Paul DeMarinis, 1/6/2019

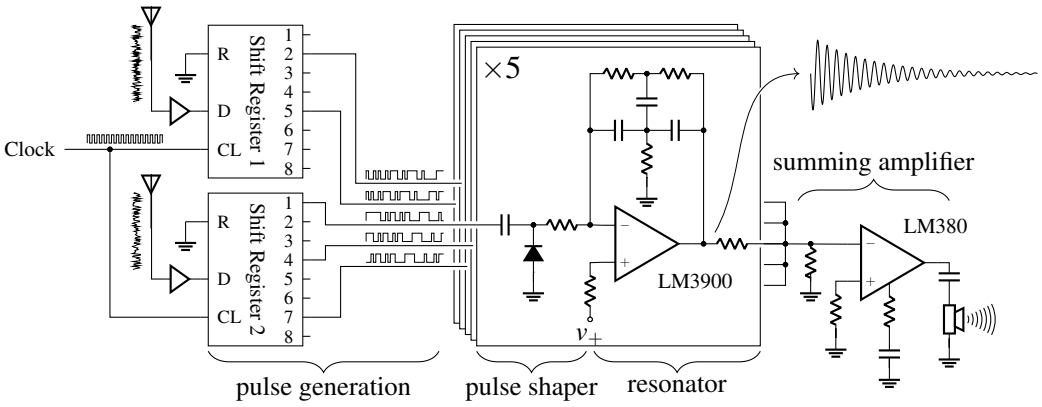

Fig. 2: The *Pygmy Gamelan* schematic, based on [1].

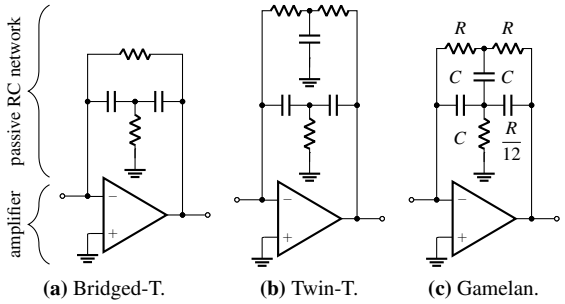

(a) Bridged-T. **(b)** Twin-T. **(c)** Gamelan.

Fig. 3: Three related active resonators.

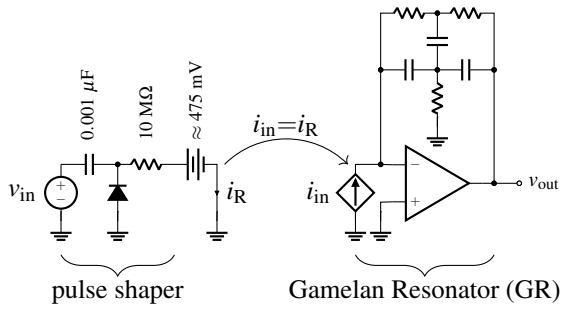

Fig. 4: Simplifying one Gamelan Resonator (GR).

paper "Simple Bandpass Filters" [16]. This publication just precedes the development of the GR, dated June-July 1973 in the short Asterisk article [1, p.47]. However, the circuits described therein are, true to the article's name, quite simple Bridged-T-based bandpass filters. One interesting facet of Burhans design is to use Q-enhancement—an active feedback path around the bandpass filter—to increase the resonance. This is similar to the technique used in the TR-808 bass drum [9, 12], but sheds little light on the GR other than pointing out that it has a relationship to Bridged-T resonators. Second, a nearly identical circuit (and its mirror image) appear in an advertisement for the graphic design firm "And Graphics" in a 1976 issue of the electronic music journal *Synapse* [17]. This, however, was published after the GR's appearance in DeMarinis' *Asterisk* article [1], so it cannot be considered a predecessor. Perhaps the two circuits have a common ancestor that remains to be found.

2.2 Separating the GR into subcircuits

We would like to set aside the details of the pulse generation, the pulse shaper, and the summing amplifier in order to analyze the GR on its own. Because each GR's amplifier can reasonably be modeled as a high-gain controlled source, the summing amplifiers and other four GR circuits will not load on it significantly: the circuit can be split at the output of each amplifier. On the input side, we notice that the large 10 MΩ resistor dominates the load looking into the GR. We notice by examining a SPICE simulation (using a component-level model of the LM3900) that the LM3900's negative terminal stays relatively fixed to a bias point, around 475 mV. So, we can reasonably model the GR's load on on the pulse shaper as simply the same large resistor and this bias voltage. Finally, the input to the GR can be modeled as an ideal controlled current source i_{in} driven by the current through the large resistor, i_R. This separation into subcircuits is shown in Fig. 4.

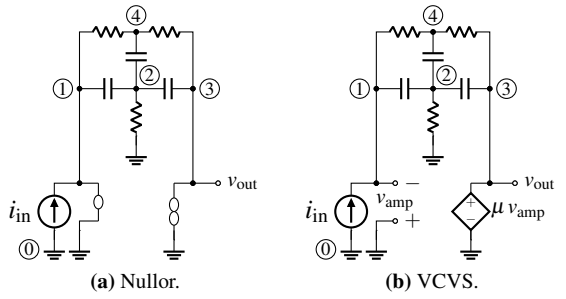

(a) Nullor. **(b)** VCVS.

Fig. 5: Two embodiments of the Gamelan resonator.

This separation into subcircuits barely affects the transient-mode behavior of the circuit at all—this has been verified by SPICE simulation. In the rest of this paper, we will consider the idealized AC analysis of the GR as it appears on the right of Fig. 4.

3 Flawed analysis with ideal amplifier

A first attempt to analyze the GR assumes that the LM3900's AC behavior can be modeled by an ideal, infinite-gain amplifier. This can be represented in circuit-theoretic terms with an idealized two-port element called a nullor, which is the combination of two idealized one-port elements: a nullator and a norator [18]. The GR with the amplifier replaced with a nullor is shown in Fig. 5a.

In investigating this configuration of the GR, we will derive its transfer function, look at its frequency response and time-domain response to an impulse, and analyze its zeros and poles.

3.1 Equation setup

Assuming ideal behavior and modeling the Norton operational amplifier as a nullor, labeling the 5 node voltages in the circuit as v_0–v_4 (with v_0 / ground as the datum node), the GR's dynamics can be described by a Modified Nodal Analysis [19] matrix equation:

$$\begin{bmatrix} G+sC & -sC & 0 & -G & 0 \\ -sC & 12G+3sC & -sC & -sC & 0 \\ 0 & -sC & G+sC & -G & +1 \\ -G & -sC & -G & 2G+sC & 0 \\ +1 & 0 & 0 & 0 & 0 \end{bmatrix} \begin{bmatrix} v_1 \\ v_2 \\ v_3 \\ v_4 \\ i_{\text{nor}} \end{bmatrix} = \begin{bmatrix} i_{\text{in}} \\ 0 \\ 0 \\ 0 \\ 0 \end{bmatrix} \tag{1}$$

where $G = 1/R$ for compactness.

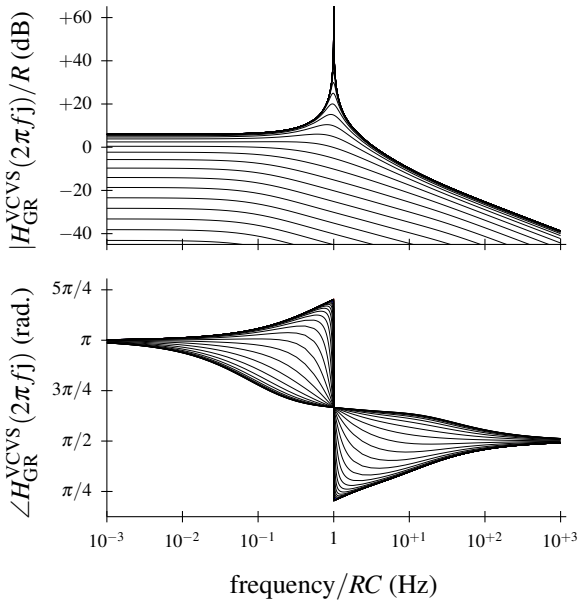

Fig. 6: A family of magnitude and phase responses of the Gamelan resonator where the Norton amplifier model is modeled using the VCVS (varying $\mu \in \{3.5 \cdot 10^{-3}, \ldots, 3.5 \cdot 10^{6}\}$: black traces, $\mu = 3500$: thick blue trace) and using the nullor (dashed red trace).

3.2 Transfer function

This can be solved (remembering that $v_{\text{out}} = v_3$) to find the transfer function $H_{\text{GR}}^{\text{ideal}}(s) = V_{\text{out}}(s)/I_{\text{in}}(s)$ as

$$H_{\text{GR}}^{\text{ideal}}(s) = -2R \frac{[R^2C^2]s^2 + 9RCs + 12}{[R^3C^3]s^3 + [4R^2C^2]s^2 + [3RC]s + 12} \tag{2}$$

By defining a scaled frequency variable $\tilde{s} = sRC$, this can be rewritten as

$$H_{\text{GR}}^{\text{ideal}}(\tilde{s}) = -2R \frac{\tilde{s}^2 + 9\tilde{s} + 12}{\tilde{s}^3 + 4\tilde{s}^2 + 3\tilde{s} + 12} \tag{3}$$

A magnitude and phase response are shown in Fig. 6 (top trace of the magnitude response and outer trace of the phase response). The magnitude response approaches $2R$ ($20\log_{10}(2R)$ dB) as $\tilde{s} \longrightarrow 0$ and 0 ($-\infty$ dB) as $\tilde{s} \longrightarrow \infty$. It has a peak at $+\infty$ ($+\infty$ dB) at $\tilde{s} = \sqrt{3} \approx 1.732$ Hz ($2\sqrt{3}\pi \approx 10.883$ rad/s). The fact that this peak goes to infinity is our first indication that this circuit is unstable.

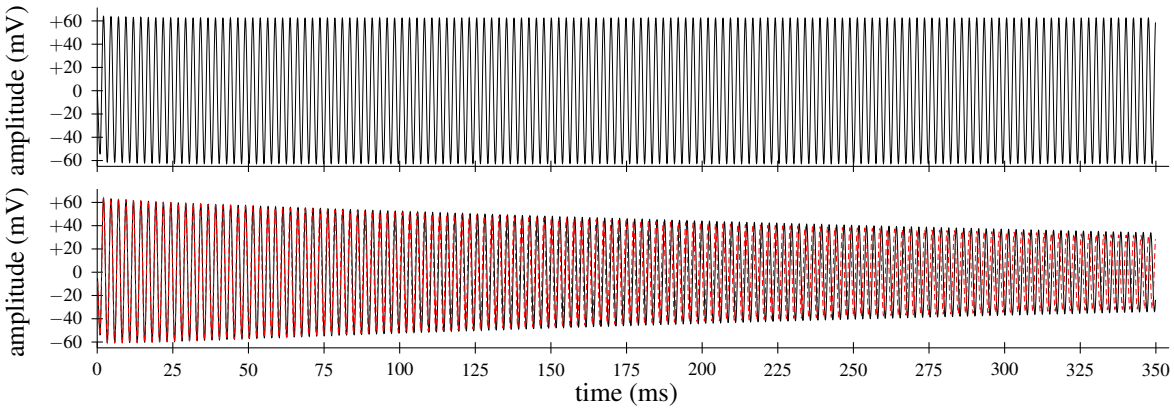

Fig. 7: Time-domain responses of the GR to a pulse (DC offset removed), including the ideal (nullor-based) Norton amplifier model (top), the full component-level Norton amplifier model (bottom, black), and the finite-gain VCVS (bottom, dashed red).

The phase response approaches $-\pi$ as $\tilde{s} \longrightarrow 0$ and $-3\pi/2$ as $\tilde{s} \longrightarrow \infty$. The phase response crosses 0 at the same frequency as the magnitude response's peak, $\tilde{s} = \sqrt{3} \approx 1.732$ Hz ($2\sqrt{3}\pi \approx 10.883$ rad/s), although is technically undefined at that point because of the pole on the imaginary axis.

3.3 Time domain response

The time-domain plot of the GR is shown as a black trace on the top panel of Fig. 7. Note that it does not closely match the simulation using a full component-level Norton amplifier model (the black trace on the bottom panel). Note also that it rings forever in response to an impulsive input: a second indication that our circuit is unstable.

For this simulation, $R = 20$ kΩ and $C = 33$ nF, giving a ≈ 406 Hz resonator (the lowest measured peak from the *Forest Booties* recording studied in §5.

3.4 Zeros

The zeros of (3) can be found by zeroing the numerator, i.e., by solving $\tilde{s}^2 + 9\tilde{s} + 12 = 0$. This can be accomplished by two distinct solutions, meaning that $H_{\mathrm{GR}}^{\mathrm{ideal}}(\tilde{s})$ has zeros at $\tilde{s} \in \{z_+, z_-\}$. These can be found using the quadratic equation by

$$z_\pm = \frac{-9 \pm \sqrt{9^2 - 4 \cdot 1 \cdot 12}}{2 \cdot 1} = \frac{-9 \pm \sqrt{33}}{2}, \quad (4)$$

giving

$$z_+ = \frac{-9 + \sqrt{33}}{2} \approx -1.627 \quad (5)$$

$$z_- = \frac{-9 - \sqrt{33}}{2} \approx -7.372. \quad (6)$$

These are both real, left-half-plane ($\Re\{z_\pm\} < 0$) zeros.

3.5 Poles

The poles of (3) can be found by zeroing the denominator, i.e., by solving $\tilde{s}^3 + 4\tilde{s}^2 + 3\tilde{s} + 12 = 0$. This is a cubic equation, and can be solved by using the techniques described in [20, 21]. Assuming a polynomial of the form $a\tilde{s}^3 + b\tilde{s}^2 + c\tilde{s} + d = 0$, we have

$$a = 1 \quad (7)$$

$$b = 4 \quad (8)$$

$$c = 3 \quad (9)$$

$$d = 12. \quad (10)$$

Using [20, 21], we get several terms from the denominator polynomial coefficients according to

$$\delta = \sqrt{\tfrac{b^2 - 3ac}{9a^2}} \quad (11)$$

$$h = 2a\delta^3 \quad (12)$$

$$s_{\mathrm{N}} = -\tfrac{b}{3a} \quad (13)$$

$$t_{\mathrm{N}} = a s_{\mathrm{N}}^3 + b s_{\mathrm{N}}^2 + c s_{\mathrm{N}} + d. \quad (14)$$

Using these gives three solutions

$$p_0 = s_N - 2\delta\left[\cosh\left(\tfrac{1}{3}\cosh^{-1}\left(\tfrac{t_N}{h}\right)\right)\right] \quad (15)$$

$$p_\pm = s_N + \delta\left[\cosh\left(\tfrac{1}{3}\cosh^{-1}\tfrac{t_N}{h}\right) \pm j\sqrt{3}\sinh\left(\tfrac{1}{3}\cosh^{-1}\tfrac{t_N}{h}\right)\right] \quad (16)$$

For our particular polynomial, we have

$$\delta = \tfrac{\sqrt{7}}{3} \approx 0.882 \quad (17)$$

$$h = \tfrac{14\sqrt{7}}{27} \approx 1.372 \quad (18)$$

$$s_N = -\tfrac{4}{3} \approx -1.333 \quad (19)$$

$$t_N = \tfrac{344}{27} \approx 12.741 \quad (20)$$

and then

$$\frac{t_N}{h} = \frac{172}{7\sqrt{7}} \approx 9.287 \quad (21)$$

and finally

$$p_0 = -4 \quad (22)$$

$$p_\pm = +j\sqrt{3} \approx \pm 1.732j\,. \quad (23)$$

These three distinct solutions mean that $H_{GR}(\tilde{s})$ has poles at $\tilde{s} \in \{p_0, p_+, p_-\}$. Both p_+ and p_- are purely imaginary; they have a real part of zero ($\Re\{p_\pm\} = 0$). Continuous-time poles with zero real part are only marginally stable, therefore this entire resonator model is only marginally stable, and technically would ring forever in response to an impulsive input. This confirms what we observed in the magnitude response and time-domain plots earlier.

We know from looking at the behavior of the circuit that the resonator should not actually marginally stable, but fully stable. As shown in Fig. 7, which shows a SPICE simulation (red trace), or as heard in *Forest Booties*, v_{out} rings but then decays in response to an impulsive input. Therefore, the model assuming an ideal amplifier, which is marginally stable, is not suitable for understanding the GR. Assuming that the resistor and capacitor values are correct as written on the schematic, an obvious candidate to explore is relaxing the assumption that the amplifier is ideal, and analyzing it with something other than a nullor.

4 Analysis with finite-gain amplifier

The LM3900 application note [22] shows that it can be appropriate, in an AC analysis, to approximate the LM3900 by a voltage-controlled voltage source (VCVS). Here we do exactly that, replacing the LM3900 with a finite-gain VCVS with a positive gain of $\mu \gg 0$. This is shown in Fig. 5b. By comparing two SPICE models of the Gamlean resonator, one using a component-level LM3900 model and one using a VCVS, we find that a value of $\mu = 3500$ matches their AC behavior. This is fairly close to what is reported in the data-sheet [23], where a chart shows a differential voltage amplification of $\approx 3000\times$ at low frequencies.

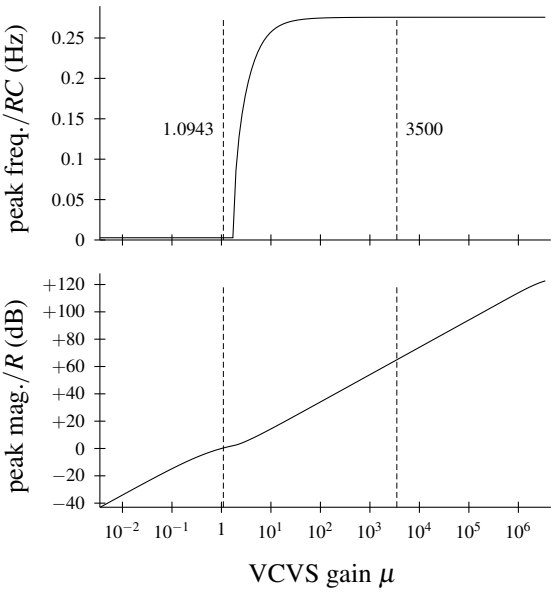

Fig. 8: Behavior of the peak frequency and amplitude of a VCVS-based model as μ varies.

4.1 Equation setup

Replacing the amplifier by a VCVS of gain μ, we can describe the GR's dynamics by a Modified Nodal Analysis [19] matrix equation:

$$\begin{bmatrix} G+sC & -sC & 0 & -G & 0 \\ -sC & 12G+3sC & -sC & -sC & 0 \\ 0 & -sC & G+sC & -G & +1 \\ -G & -sC & -G & 2G+sC & 0 \\ -\mu & 0 & +1 & 0 & 0 \end{bmatrix} \begin{bmatrix} v_1 \\ v_2 \\ v_3 \\ v_4 \\ i_{amp} \end{bmatrix} = \begin{bmatrix} i_{in} \\ 0 \\ 0 \\ 0 \\ 0 \end{bmatrix} \quad (24)$$

where, as before, $G = 1/R$ for compactness.

4.2 Transfer function

Our reason to study the behavior of the GR as a function of μ, despite the fact that the original device has a fixed μ, is that future designers may be interested in building on this type of circuit, and we would like to

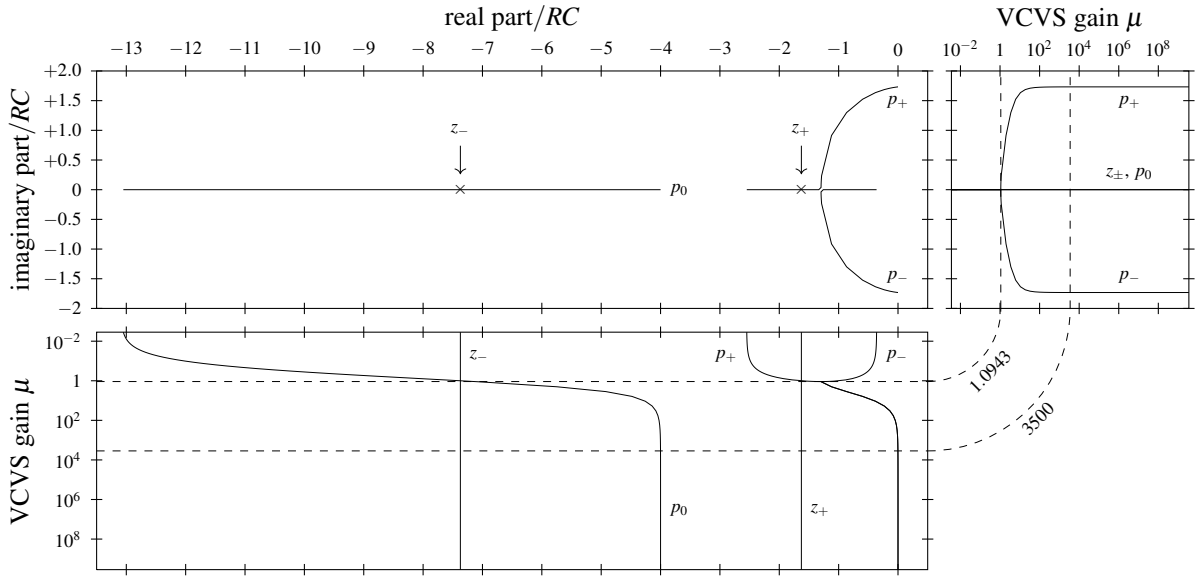

Fig. 9: Poles and zeros of the GR, modeling the Norton amplifier as a voltage-controlled voltage source of gain μ. The upper left pan shows the loci on the complex plane; the upper right pane shows the imaginary part dependence on μ; and the lower left pan shows the real part dependence on μ. Dashed lines and mark the position of the loci where $\mu = 3500$ (the approximation to the component-level SPICE model) and $\mu \approx 1.0943$ (the critical value where the poles $p_\pm$ split).

give some insight to how it functions with different amplifier gains.

As before, the above matrix equations is solved (remembering that $v_{\text{out}} = v_3$) to find the transfer function $H_{GR}^{\text{VCVS}}(s) = V_{\text{out}}(s)/I_{\text{in}}(s)$ as

$$H_{\text{GR}}^{\text{VCVS}}(s) = -2R\left(\tfrac{\mu}{\mu+1}\right)\frac{R^2C^2s^2+9RCs+12}{R^3C^3s^3+4\frac{\mu+4}{\mu+1}R^2C^2s^2+3\frac{\mu+13}{\mu+1}RCs+12}\,. \quad (25)$$

By again defining a scaled frequency variable $\tilde{s} = sRC$, this can be rewritten as

$$H_{\text{GR}}^{\text{VCVS}}(\tilde{s}) = -2R\left(\tfrac{\mu}{\mu+1}\right)\frac{\tilde{s}^2+9\tilde{s}+12}{\tilde{s}^3+4\frac{\mu+4}{\mu+1}\tilde{s}^2+3\frac{\mu+13}{\mu+1}\tilde{s}+12}\,. \quad (26)$$

Notice that as $\mu \longrightarrow \infty$, this reduces to the transfer function using a nullor, as in (3). This now allows us to study the magnitude response and pole and zero locations as a function of μ.

A family of magnitude and phase responses as μ varies are given in Fig. 6. The peak frequency and magnitude are measured and presented as a function of μ in Fig. 8. The peak gain increases somewhat smoothly as a function of μ, and the peak frequency varies more dramatically as μ gets small. Notice that the peak frequency is relatively stable around the actual amplifier value of $\mu = 3500$.

4.3 Time domain response

A time domain simulation of the circuit with $\mu = 3500$ is shown in the bottom panel of Fig. 7, with the dashed red trace. Notice that it's almost identical to the trace from the model with the full component-level Norton amplifier, verifying that our earlier simplification—splitting the circuit into a pulse shaper and a resonator, to ease analysis—is justified.

4.4 Zeros

The zeros of $H_{\text{GR}}^{\text{VCVS}}(s)$ are identical to those of $H_{\text{ideal}}^{\text{VCVS}}(s)$, as shown in §3.4. Note well that neither of the two zeros depend in any way on μ. The zeros are shown on Fig. 9.

4.5 Poles

The poles come from zeroing the denominator polynomial, i.e., by solving $\tilde{s}^3 + 4\frac{\mu+4}{\mu+1}\tilde{s}^2 + 3\frac{\mu+13}{\mu+1}\tilde{s} + 12 = 0$. Again assuming a polynomial of the form $a\tilde{s}^3 + b\tilde{s}^2 + c\tilde{s} + d = 0$, we have

$$a = 1 \quad (27)$$

$$b = 4\frac{\mu+4}{\mu+1} \tag{28}$$

$$c = 3\frac{\mu+13}{\mu+1} \tag{29}$$

$$d = 12\,. \tag{30}$$

For our polynomial, we find the terms

$$\delta = \frac{\sqrt{7\mu^2+2\mu+139}}{3(\mu+1)} \tag{31}$$

$$h = \frac{2(7\mu^2+2\mu+139)^{3/2}}{27(\mu+1)^3} \tag{32}$$

$$s_{\mathrm{N}} = -\frac{4\mu+16}{3\mu+3} \tag{33}$$

$$t_{\mathrm{N}} = \frac{4(86\mu^3+141\mu^2-84\mu+725)}{27(\mu+1)^3}\,. \tag{34}$$

The important factor t_{N}/h is

$$\frac{t_{\mathrm{N}}}{h} = \frac{2(86\mu^3+141\mu^2-84\mu+725)}{(7\mu^2+2\mu+139)^{3/2}}\,. \tag{35}$$

The limit of t_{N}/h as $\mu \longrightarrow 0$ is $\frac{1450}{139\sqrt{139}} \approx 0.8848$.

The limit of t_{N}/h as $\mu \longrightarrow \infty$ is $\frac{172}{7\sqrt{7}} \approx 9.2871$.

Since μ is the gain of the amplifier, ideally $\mu \longrightarrow \infty$, we would expect $1 \ll \mu$. For that reason, we can focus only on the case of $t_{\mathrm{N}}/h > 1$, considering the other cases to be very unrealistic for any reasonable amplifiers. Still, the two cases for $t_{\mathrm{N}}/h \leq 1$ are given for completeness. The poles are shown on Fig. 9

4.5.1 Case 1: one real root and two complex conjugate roots

When $t_{\mathrm{N}}/h > 1$ (corresponding to $1.0943 < \mu$), we have three distinct poles: one real pole (p_0) and two complex conjugate poles ($p_\pm$, where $\Im\{p_+\} = -\Im\{p_-\}$, $\Re\{p_+\} = \Re\{p_-\}$)). They are all negative ($\Re\{p_{\{\pm,0\}}\} < 0$) and hence stable. Two are complex conjugates. Note that the estimated voltage gain for the circuit is $\mu \approx 3500$, which is well into this range because $1.0943 \ll 3500$. Therefore, Case 1, which is also the only case to involve the characteristic ringing behavior of the circuit due to the complex conjugate poles, is by far the most important case. The poles are found as before, giving

$$p_0 = s_{\mathrm{N}} - 2\delta\left[\cosh\left(\tfrac{1}{3}\cosh^{-1}\left(\tfrac{t_{\mathrm{N}}}{h}\right)\right)\right] \tag{36}$$

$$p_\pm = s_{\mathrm{N}} + \delta\left[\cosh\left(\tfrac{1}{3}\cosh^{-1}\tfrac{t_{\mathrm{N}}}{h}\right) \pm \mathrm{j}\sqrt{3}\sinh\left(\tfrac{1}{3}\cosh^{-1}\tfrac{t_{\mathrm{N}}}{h}\right)\right]. \tag{37}$$

4.5.2 Case 2: three real roots, two of which are equal

When $t_{\mathrm{N}}/h = 1$ (corresponding to $\mu \approx 1.0943$), the two poles $p_\pm$ become coincident on the real axis at $p_\pm = -1.2976$, while $p_0 \approx -7.1364$. At this point, any oscillations would cease, and the GR would just "thump" rather than ring. Again, all three poles are negative, and hence stable.

4.5.3 Case 3: three distinct real roots

When $t_{\mathrm{N}}/h < 1$ (corresponding to $0 < \mu < 1.0943$), the poles are all real and distinct. Again, all three roots are negative, and hence stable. Here, it is a little nicer to look at the pole expressions as [20]

$$p_0 = s_{\mathrm{N}} + 2\delta\cos\left[\tfrac{1}{3}\arccos\left(-t_{\mathrm{N}}/h\right) + \tfrac{2}{3}\pi\right] \tag{38}$$

$$p_+ = s_{\mathrm{N}} + 2\delta\cos\left[\tfrac{1}{3}\arccos\left(-t_{\mathrm{N}}/h\right) - \tfrac{2}{3}\pi\right] \tag{39}$$

$$p_- = s_{\mathrm{N}} + 2\delta\cos\left[\tfrac{1}{3}\arccos\left(-t_{\mathrm{N}}/h\right)\right]\,. \tag{40}$$

5 Transfer function use in component value estimation based on recording

Although our transfer function (26) is not parametrized, it is enough to allow for the systematic testing of standard component values versus recorded resonance peaks in order to experimentally determine which values are likely to have been used in the circuit that was used in those recordings.

In the original study of the circuit [6], the 1978 *Forest Booties* recording was analysed to determine the resonant peak frequencies of each of the five filters included in that first generation circuit. These peaks were: 406 Hz, 833 Hz, 946 Hz, 1166 Hz, and 1465 Hz. Considering component values from the pre-1977 IEC 60063 standard series [24][4], we tested every possible combination of R and C, finding the pair that produces a resonant peak closest to each measured peak. Fig. 10 shows magnitude responses for these peaks along with the corresponding resistance and capacitance values, alongside dotted lines representing the measured frequencies of the peaks.

[4] For details on standard series values see [25].

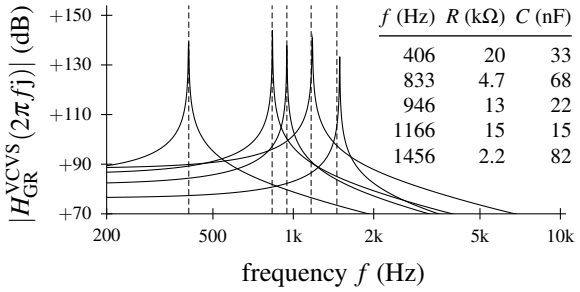

Fig. 10: Magnitude responses with closest peaks to those measured in *Forest Booties*.

6 Comments on digital modeling

Given the simplification into two parts shown in Fig. 4, and our derivation of the transfer function, several virtual analog approaches would be appropriate for making a digital model of the GR. The GR can be modeled by using the bilinear transform or other s-to-z mappings to discretize the transfer function [26], or by modeling the circuit as a wave digital filter [27, 12]. The pulse shaper resembles a common diode clipper circuit, so can be modeling in a number of ways, including ad hoc modeling along the lines of [9, 10, 11], as a wave digital filter with a single nonlinearity [28, 29, 30, 12], using state space modeling [31, 29, 32], or using Port Hamiltonian modeling [33].

7 Conclusion

In this paper, we gave an analysis of the unique resonator used in Paul DeMarinis' *Pygmy Gamelan*, which we call the *Gamelan Resonator*. It is somewhat related to the Bridged-T and Twin-T networks, but the particular topology (and relationships of component values, particularly the peculiar $R/12$) seem to be unique. We derived its transfer function, showed the magnitude and phase response, and found zeros and poles for two ways of modeling the Norton amplifier: 1) as an ideal amplifier (nullor) and 2) as a voltage-controlled voltage source (VCVS). We showed that the nullor model is only marginally stable, and hence unsuitable for modeling the circuit. Interestingly, the circuit must be analyzed with a non-ideal amplifier (e.g., our VCVS) to gives sensible behavior. This allows us to graph an accurate magnitude response, which shows that the GR, analyzed as a current-to-voltage impedance transfer function $H_{GR}(s) = V_{out}(s)/I_{in}(s)$, is an original kind of 3rd-order resonant lowpass filter.

DeMarinis' schematic and recording were enough to implement a Pure Data ersatz [6], but the present analysis allows for the development of models which more accurately embody the originality of this project down to the component level (§6). Even though artist-engineers such as DeMarinis "experimented (...) by curiosity and blind error,"[5] they also developed original systems such as the GR, in which component-level decisions represent both careful artistic choices and technical innovations. Alongside [6], we see this paper as a step towards considering "circuitry's significance for the musical, sonic, and textural sciences that are imagined alongside the unit," [34] because they help us situate DeMarinis' experiments and perspectives in the wider context of arts and engineering research.

Acknowledgments

Thank you to Paul DeMarinis for invaluable insight on his project, to Fabian Esqueda for helpful advice on Norton amplifiers, and to the Nora Eccles Harrison Museum staff for facilitating our use of their image.

References

[1] DeMarinis, P., "The Pygmy Gamelan," *Asterisk: J. New Music*, 1(2), pp. 46–48, 1975.

[2] Pritikin, R., "Interview with Paul DeMarinis," *Art Practical*, 3(13), 2012.

[3] Chiba, S.-I., "Interview with Paul DeMarinis," 1997, `https://web.archive.org/web/20171022031024/http://www.lovely.com/press/articles/interview.demarinis.japan.html`, accessed May 27, 2020.

[4] Turner, F., *Paul DeMarinis: Buried in Noise*, chapter "The Pygmy Gamelan as technology of consciousness", pp. 22–31, Kehrer Verlag, Heidelberg, Germany, 2010.

[5] Ouzounian, G., "An Interview with Paul DeMarinis," *Comput. Music J.*, 34(4), pp. 10–21, 2010.

[6] Teboul, E. J., *A Method for the Analysis of Handmade Electronic Music as the Basis of New Works*, Ph.D diss., Rensselaer Polytechnic Inst., Troy, NY, 2020.

[7] DeMarinis, P., "Circuits," n.d., `https://pauldemarinis.org/Circuits.html`, accessed December 13, 2018.

[5] Email with Paul DeMarinis, 6/4/2019.

[8] DeMarinis, P., *If God Were Alive (& He Is) You Could Reach Him By Telephone / Forest Booties*, LP record VR106, New York: Vital Records, 1980.

[9] Werner, K. J., Abel, J. S., and Smith III, J. O., "A physically-informed, circuit-bendable, digital model of the Roland TR-808 bass drum circuit," in *Proc. 17th Int. Conf. Digital Audio Effects*, pp. 159–166, Erlangen, Germany, 2014.

[10] Werner, K. J., Abel, J. S., and Smith, J. O., "More cowbell: A physically-informed, circuit-bendable, digital model of the TR-808 cowbell," in *Proc. 137th Conv. Audio Eng. Soc.*, Los Angeles, CA, 2014, Conv. Paper #9207.

[11] Werner, K. J., Abel, J. S., and Smith III, J. O., "The TR-808 cymbal: A physically-informed, circuit-bendable, digital model," in *Proc. Joint Session Int. Comput. Music Conf. / Sound Music Comput. Conf.*, pp. 1453–1460, Athens, Greece, 2014.

[12] Werner, K. J., *Virtual Analog Modeling of Audio Circuitry Using Wave Digital Filters*, Ph.D. diss., Stanford Univ., CA, 2016.

[13] Zobel, O. J., "Distortion correction in electrical circuits with constant resistance recurrent networks," *Bell Syst. Tech. J.*, 7(3), pp. 438–534, 1928.

[14] Sinclair, D. B., "The twin-T: A new type of null instrument for measuring impedance at frequencies up to 30 megacycles," *Proc. IRE*, 28(7), pp. 310–318, 1940.

[15] Stinchcombe, T. E., "The Serge VCS: How It Works," *EContact! J. Canadian Electroacoustic Community*, 17(4), 2016.

[16] Burhans, R. W., "Simple bandpass filters," *J. Audio Eng. Soc.*, 21(4), pp. 275–277, 1973.

[17] "Composer/Performer," *Synapse Mag.*, 1(4), p. 6, 1976.

[18] Carlin, H. J., "Singular network elements," *IEEE Trans. Circuit Theory*, 11(1), pp. 67–72, 1964.

[19] Ho, C.-W., Ruehli, A. E., and Brennan, P. A., "The modified nodal approach to network analysis," *IEEE Trans. Circuits Syst.*, 22(6), pp. 504–509, 1975.

[20] Nickalls, R. W. D., "A new approach to solving the cubic: Cardan's solution revealed," *Math. Gazette*, 77(480), pp. 354–359, 1993.

[21] Holmes, G. C., "The use of hyperbolic cosines in solving cubic polynomials," *Math. Gazette*, 86(507), pp. 473–477, 2002.

[22] National Semiconductor, "The LM3900: A new current-differencing quad of $\pm$ amplifiers," App. Note AN-72, 1972.

[23] Texas Instruments, "LM2900, LM3900 Quadruple Norton Operational Amplifiers," Technical Report SLOS059, Dallas, TX, 1979, rev. Sept. 1990.

[24] I.E.C., "60063: Preferred number series for resistors and capacitors. Second edition (1963) incorporating Amendments No. 1 (1967) and No. 2 (1977)," 1963.

[25] van der Salm, S. A. M., "Renard's Preferred Numbers," *J. Oughtred Soc.*, 13(1), pp. 44–53, 2004.

[26] Germain, F. G. and Werner, K. J., "Design principles for lumped model discretisation using Möbius transforms," *Proc. 18th Int. Conf. Digital Audio Effects*, 2015.

[27] Fettweis, A., "Wave Digital Filters: Theory and Practice," *Proc. IEEE*, 74(2), pp. 270–327, 1986.

[28] Meerkötter, K. and Scholz, R., "Digital simulation of nonlinear circuits by wave digital filter principles," in *IEEE Int. Symp. Circuits Syst.*, pp. 720–723, Portland, OR, 1989.

[29] Yeh, D. T., *Digital Implementation of Musical Distortion Circuits by Analysis and Simulation*, Ph.D. diss., Stanford Univ., CA, 2009.

[30] Werner, K. J., Nangia, V., Bernardini, A., Smith III, J. O., and Sarti, A., "An improved and generalized diode clipper model for wave digital filters," in *Proc. 139th Conv. Audio Eng. Soc.*, New York, NY, 2015.

[31] Yeh, D. T., Abel, J. S., Vladimirescu, A., and Smith, J. O., "Numerical Methods for Simulation of Guitar Distortion Circuits," *Comput. Music J.*, 32(2), pp. 23–42, 2008.

[32] Holters, M. and Zölzer, U., "A generalized method for the derivation of non-linear state-space models from circuit schematics," in *Proc. Europ. Signal Process. Conf.*, Nice, France, 2015.

[33] Müller, R. and Hélie, T., "Fully-implicit algebro-differential parametrization of circuits," in *Proc. 23rd Int. Conf. Digital Audio Effects*, pp. 78–85, Vienna, Austria, 2020.

[34] McKittrick, K. and Weheliye, A. G., "808s and Heartbreak," *Propter Nos*, 2(1), pp. 13–42, 2017.